Check for updates

Mechanism guided two-electron energy storage for redox-flow batteries using nickel bis(diphosphine) complexes†

Md. Musharraf Hossain and Byron H. Farnum [ID] *

The storage of multiple electrons per molecule can greatly enhance the energy density of redox-flow batteries (RFBs). Here, we show that nickel bis(diphosphine) complexes efficiently store multiple electrons through either sequential 1e⁻ redox waves or a concerted 2e⁻ redox wave, depending on their coordination environment. Mechanistic studies comparing ligand sterics (−Me *vs.* −Ph) and coordination of monodentate ligands (MeCN *vs.* Cl⁻) allow for selective control of the electron transfer pathway, steering electron storage toward the more favorable 2e⁻ wave. Continuous charge–discharge cycling experiments show more negative charge–discharge potentials and improved capacity retention in the presence of Cl⁻, thus improving the energy storage of nickel bis(diphosphine) complexes as anolytes in RFBs. This work shows how mechanistic understanding of 2e⁻ redox cycles for transition metal complexes can create new opportunities for multi-electron storage in RFBs.

Renewable energy resources (*i.e.* solar and wind) are now prime targets to address the global energy crisis.[1] However, existing solar and wind power plants still have limited impact on grid systems because of their intermittent nature. Therefore, significant efforts are being made to develop efficient grid-scale energy storage (GSES) systems to improve grid flexibility.[2] Redox-flow batteries (RFBs) are among the best candidates to solve these challenges.

RFBs are regarded as one of the most practical options for energy storage applications on medium and large-scale.[2–12] Their unique architecture utilizes storage tanks filled with redox-active electrolytes wherein their power rating (kW) is a function of the electrode size and the number of cells in a stack while their energy storage capacity (kW h) is dependent on the cell voltage and concentration of active species. The independent control of power and capacity provides design flexibility,

Department of Chemistry and Biochemistry, Auburn University, Auburn, AL 36849, USA. E-mail: farnum@auburn.edu

† Electronic supplementary information (ESI) available: Experimental procedures, NMR, ESI-MS, UV-vis spectra, and cyclic voltammetry. See DOI: https://doi.org/10.1039/d4cc06547f

ensuring long cycling and inherent safety for GSES applications.

Due to the inherently low energy density of RFBs, research efforts have focused on the storage of multiple electrons per redox-active molecule. This can be achieved either through sequential redox reactions of a molecule where each electron is stored at a unique potential, or through a concerted multi-electron redox reaction in which multiple electrons are stored at the same potential. The former can result in significant changes in the cell voltage of the RFB if the separation in potentials is large, whereas the latter strategy ensures that all electrons are stored equally, yielding a consistent cell voltage.

Achieving reversible multi-electron redox reactions, however, is challenging and requires intimate knowledge of electron transfer mechanisms. For organic molecules, reversible multi-electron reactions are often achieved through proton-coupled electron transfer (PCET) reactions where proton transfer is key to balancing charge and realizing a multi-electron path.[10,11] Inorganic transition metal complexes, however, require changes in the coordination environment to achieve multi-electron redox activity.[13–16] Known examples of this class use ligand coupled electron transfer (LCET) to cycle between complexes of higher coordination in the oxidized state and lower coordination in the reduced state.

Here, we report a mechanistic study on the 2e⁻ redox cycle of Ni(II) bis(diphosphine) complexes, commonly explored as proton-reduction catalysts,[17–20] and show these molecules work effectively as anolytes for multi-electron storage RFBs. Furthermore, we show that the inclusion of Cl⁻ in the coordination environment around the nickel center allows for selective control of the multi-electron redox cycle, switching between sequential 1e⁻ storage and concerted 2e⁻ storage.

The chemical structures of $[Ni(dmpe)_2]^{2+}$ and $[Ni(dppe)_2]^{2+}$, where dmpe is 1,2-bis(dimethylphosphino)ethane and dppe is 1,2-bis(diphenylphosphino)ethane are shown in Fig. 1a and d along with their corresponding cyclic voltammograms (CV) obtained in MeCN with 1 mM of each complex (Fig. 1b and e). Using 0.2 M TBAPF₆ electrolyte, $[Ni(dmpe)_2]^{2+}$ displays a
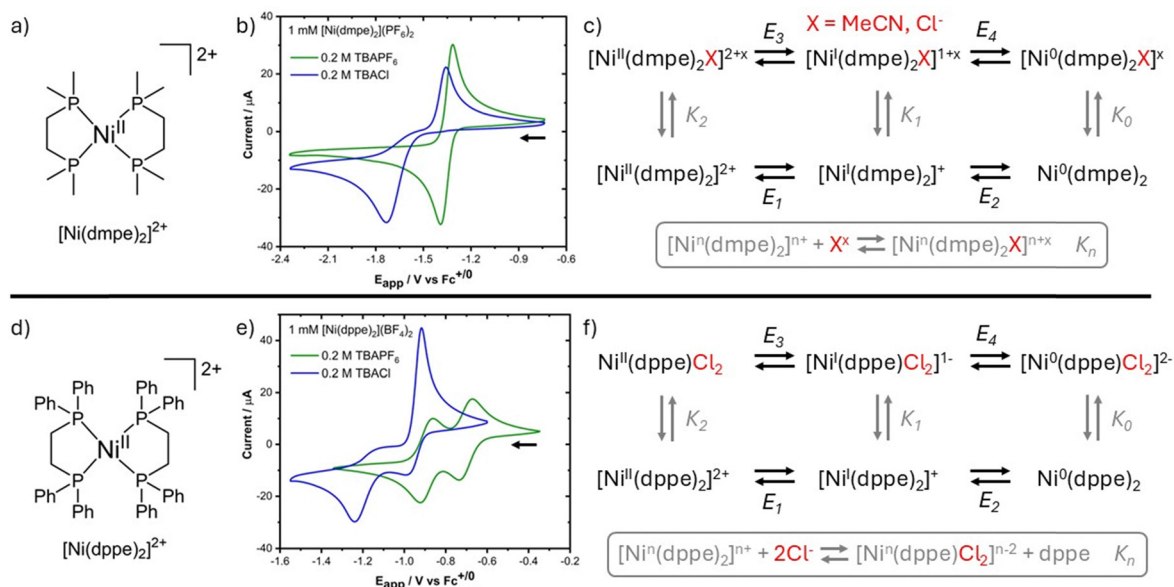
Fig. 1 (a) and (d) Chemical structures of $[Ni(dmpe)_2]^{2+}$ and $[Ni(dppe)_2]^{2+}$. (b) and (e) CV data obtained for 1 mM $[Ni(dmpe)_2](PF_6)_2$ or 1 mM $[Ni(dppe)_2](BF_4)_2$ in MeCN with different electrolytes: 0.2 M TBAPF$_6$ or 0.2 M TBACl (scan rate: 0.1 V s^{-1}, arrow indicates initial scanning direction). (c) and (f) Thermochemical cycles describing the array of electron transfer and ligand transfer reactions which give rise to 2e$^-$ or 1e$^-$ redox activity.

single 2e$^-$ Ni(II/0) redox wave with $E_{\frac{1}{2}} = -1.36$ V *vs.* Fc$^{+/0}$, while $[Ni(dppe)_2]^{2+}$ displays two sequential 1e$^-$ redox waves with $E_{\frac{1}{2}} = -0.69$ V and –0.89 V *vs.* Fc$^{+/0}$ assigned to Ni(II/I) and Ni(I/0) redox couples. The 2e$^-$ behavior observed for $[Ni(dmpe)_2]^{2+}$ arises from the coordination of MeCN to Ni(II), thus forming $[Ni(dmpe)_2(MeCN)]^{2+}$ in MeCN solution (Fig. S12a, ESI†). This coordination pushes the Ni(II/I) reduction potential in a negative direction and generates a state of potential inversion between the Ni(II/I) and Ni(I/0) redox couples (*i.e.* Ni(II/I) < Ni(I/0)), producing a 2e$^-$ redox wave in the CV. In the case of the $[Ni(dppe)_2]^{2+}$, coordination of MeCN to Ni(II) does not occur (Fig. S12b, ESI†) and thus the reduction of Ni(II) to Ni(0) occurs in a sequential fashion with the normal potential ordering of Ni(II/I) > Ni(I/0).

These redox mechanisms are summarized by the thermochemical cycles shown in Fig. 1. Reduction of $[Ni(dppe)_2]^{2+}$ occurs *via* a sequential 1e$^-$ path corresponding to reduction at E_1 followed by reduction at E_2 (Fig. 1f). However, the coordination of MeCN to $[Ni(dmpe)_2]^{2+}$ shifts the Ni(II/I) reduction potential according to the equilibrium constant K_2, resulting in a new value E_3. Following reduction to $[Ni(dmpe)_2(MeCN)]^+$, the MeCN ligand dissociates ($1/K_1$), returning the structure to a four-coordinate environment where Ni(I) is reduced to Ni(0) at E_2. This reduction sequence ($E_3 \rightarrow 1/K_1 \rightarrow E_2$) represents an ECE cycle where E is an electron transfer step and C is a chemical step (*i.e.* ligand transfer) and is common for 2e$^-$ transfer reactions. Oxidation of Ni(0) back to Ni(II) occurs in reverse order and yields a reversible CV wave.

The specific reason for the favorability of the ECE path in $[Ni(dmpe)_2]^{2+}$ lies in the ability to change its coordination environment as a function of oxidation state. $[Ni(dmpe)_2]^{2+}$ can be isolated as a square planar structure but adopts square

pyramidal in solution due to MeCN coordination.[17] The d^8 Ni(II) center is able to accommodate the five-coordinate environment to yield an 18 electron complex, but reduction to the d^9 Ni(I) and d^{10} Ni(0) strongly disfavors five-coordinate geometries due to the result of 19 and 20 electron complexes, respectively. Steric hindrance by the phenyl groups of $[Ni(dppe)_2]^{2+}$ disrupts MeCN coordination and prevents the 2e$^-$ ECE cycle from being observed.

Given the differences in CV data observed for the two complexes as a result of MeCN coordination (or lack thereof), electrochemical experiments were also performed in the presence of Cl$^-$ to further study the impact of monodentate coordination on their redox cycles. Overlaid in Fig. 1b and e are CVs collected in MeCN with 0.2 M TBACl as the electrolyte. In the case of $[Ni(dmpe)_2]^{2+}$, the cathodic peak was shifted -330 mV to $E_{pc} = -1.73$ V while the anodic peak was relatively unchanged ($E_{pa} = -1.35$ V) with respect to 0.2 M TBAPF$_6$ electrolyte (Table S2, ESI†). For $[Ni(dppe)_2]^{2+}$, the two cathodic peaks were shifted by -260 mV and -330 mV to $E_{pc} = -0.98$ V and -1.25 V, respectively. Furthermore, the anodic peaks were consolidated mostly into a single oxidation peak at $E_{pa} = -0.92$ V with a much smaller peak observed at $E_{pa} = -1.14$ V.

Changes observed for both complexes are ascribed to coordination and dissociation of Cl$^-$ as a function of oxidation state. UV-visible absorption studies showed Cl$^-$ coordination to both $[Ni(dmpe)_2]^{2+}$ and $[Ni(dppe)_2]^{2+}$ (Fig. S13 and S14, ESI†), however, with different resulting complexes. In the case of $[Ni(dmpe)_2]^{2+}$, the coordination of Cl$^-$ yields a 1:1 complex, $[Ni(dmpe)_2Cl]^+$, and shifts the redox potentials further into an inverted state by increasing K_2 (and thus shifting E_3) resulting in the same ECE pathway for the reduction and oxidation processes observed in the absence in Cl$^-$.

Coordination of Cl^- to $[Ni(dppe)_2]^{2+}$, however, results in a $2:1$ complex, $Ni(dppe)Cl_2$, wherein one dppe ligand is dissociated. UV-vis and electrochemical comparisons with independently obtained $Ni(dppe)Cl_2$ verified this result (Fig. S14 and S16, ESI†). Using Fig. 1f as reference, the reduction of Ni(II) to Ni(0) for the new $Ni(dppe)Cl_2$ starting complex occurs via $E_3 \rightarrow E_4 \rightarrow 1/K_0$ (EEC) while oxidation of Ni(0) back to Ni(II) occurs via $E_2 \rightarrow K_1 \rightarrow E_3$ (ECE). These cycles can be gleaned from the appearance of two shifted cathodic waves corresponding to reduction at E_3 and E_4 while the oxidation process shows a single anodic peak. Notably, the Ni(0) complex is assigned to $Ni(dppe)_2$ in which the reaction $1/K_0$ involves ligand exchange between Cl^- and dppe. We believe this is due to better stabilization of the Ni(0) state by the π-acceptor dppe ligand, rather than the π-donor Cl^-. Control experiments in which excess dppe ligand was added to a $Ni(dppe)Cl_2$ electrolyte solution found identical CV behavior as was obtained for excess Cl^- in $[Ni(dppe)_2]^{2+}$ solution (Fig. S16, ESI†), thus confirming the formation of $Ni(dppe)_2$ at the Ni(0) state. The differing pathways for reduction and oxidation (EEC vs. ECE) is due to the relatively slow kinetics for ligand transfer between Cl^- and dppe at the Ni(I) state. This kinetic argument is supported by CVs which show that peak potentials and peak currents change as a function of scan rate, indicating that Cl^-/dppe ligand transfer occurs on the same time scale as the scan rate (Fig. S16, ESI†).

To fully evaluate the suitability of $[Ni(dmpe)_2]^{2+}$ and $[Ni(dppe)_2]^{2+}$ as anolytes in RFBs, it is essential to investigate the complete charging and discharging of Ni(II/0) redox couples over an extended number of cycles. Extended CV cycling of

nickel complexes in both electrolytes indicated no significant current loss, suggesting chemically reversible redox cycles. However, some nickel bis(diphosphine) complexes have been observed to decompose to nickel nanoparticles in the reduced state, resulting in chemically irreversible CVs following multiple cycles.[19] This observation was not found in the present molecules.

Charge–discharge cycling was performed for each complex for 25 cycles in a three-electrode electrochemical H-cell with carbon felt electrodes and 5 mM ferrocene in the catholyte chamber. Fig. 2a and b shows the complete charge–discharge cycling along with comparisons of the 2nd cycle for 1 mM $[Ni(dmpe)_2]^{2+}$ in MeCN with either 0.2 M $TBAPF_6$ or 0.2 M TBACl as the supporting electrolyte. Fig. 2c shows the capacity retention and coulombic efficiency measured for each cycle as a function of electrolyte conditions. In the case of 0.2 M $TBAPF_6$ electrolyte, the initial charge capacity was 0.53 mAh, corresponding to $1.96e^-$ per molecule; however, the capacity faded rapidly with increased cycle numbers, as seen by the compression of the data in time for Fig. 2a, losing 3.9%/cycle over the first 10 cycles and slowing to 2.3%/cycle for cycles 10–25. When TBACl was used as the supporting electrolyte, the initial capacity was the same as $TBAPF_6$ at 0.52 mAh ($1.93e^-$ per molecule), but the capacity fade rate decreased to 1.4%/cycle (Fig. 2c). We believe that the decrease in capacity fade is the result of more efficient conversion of $[Ni(dmpe)_2]^+$ to $Ni(dmpe)_2Cl$, resulting in a more complete ECE oxidation cycle. The charge–discharge potential also shifted negatively in the presence of Cl^-, from -1.39 V with $TBAPF_6$ to -1.50 V with TBACl, matching our results from CV experiments. This change in potential results
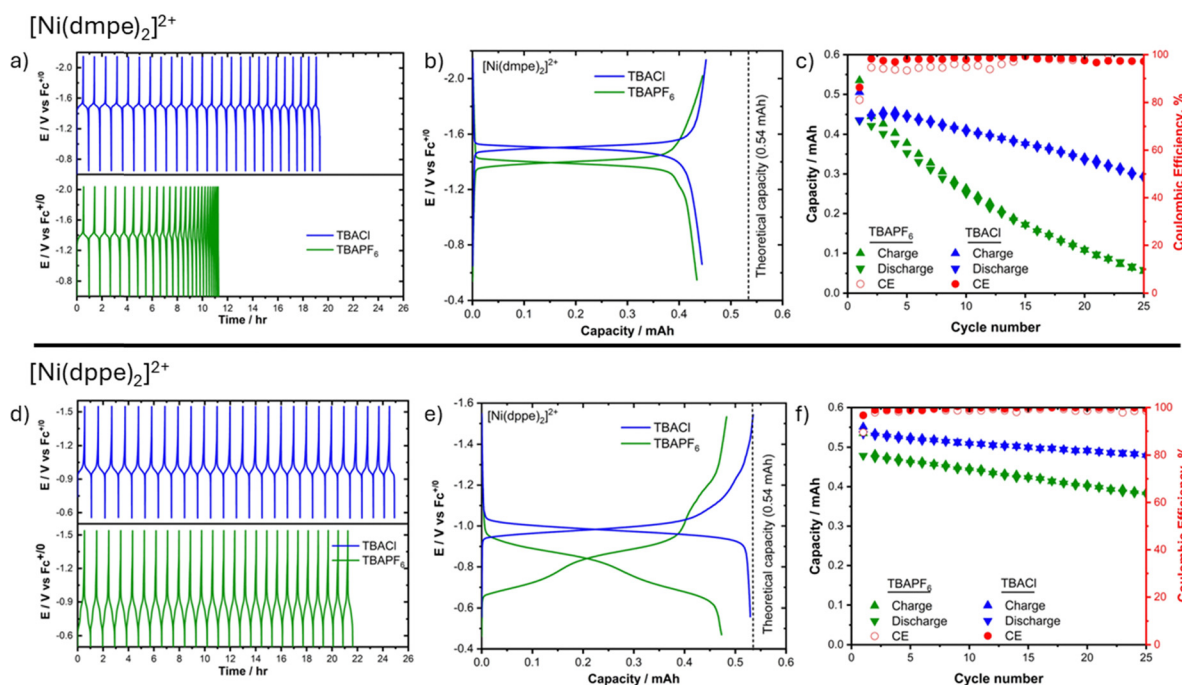

Fig. 2 (a) and (d) Representative charge–discharge voltage vs. time data for either 1 mM $[Ni(dmpe)_2](PF_6)_2$ or 1 mM $[Ni(dppe)_2](BF_4)_2$ in MeCN with 0.2 M $TBAPF_6$ (green) or 0.2 M TBACl (blue) electrolyte. Charging current = discharging current = 1 mA. (b) and (e) Comparison of the 2nd charge–discharge cycle for each complex in each electrolyte. (c) and (f) Capacity and coulombic efficiency vs. cycle number for each complex in each electrolyte.

in a higher stored voltage when paired with the ferrocene catholyte in a two-electrode cell.

Chronopotentiometric cycling experiments performed using 1 mM $[Ni(dppe)_2]^{2+}$ in different electrolyte conditions (Fig. 2d–f) showed similar improvements to the capacity fade rate in the presence of Cl^-, decreasing from 0.76%/cycle in $TBAPF_6$ to 0.38%/cycle in TBACl. Overall, the capacity fade rate was much lower for $[Ni(dppe)_2]^{2+}$ than $[Ni(dmpe)_2]^{2+}$ in both electrolytes, indicating higher stability despite the more complex ligand transfer steps. Most importantly, the presence of Cl^- consolidated the two distinct charging-discharge voltage plateaus observed in $TBAPF_6$ into a single plateau consistent with a $2e^-$ process. The new $2e^-$ charge–discharge voltage was shifted -150 mV with respect to the sequential $1e^-$ path and achieved a higher charging capacity (0.54 mA h, $2e^-$ per molecule). Both results represent an increase in the energy storage density in the context of an RFB.

The voltage observed in the presence of Cl^- is consistent with the first cathodic peak from CV experiments ($E_{pc} = -0.98$ V). We therefore believe the $2e^-$ charge–discharge behavior is due to efficient ligand transfer between Cl^- and dppe, converting $[Ni(dppe)Cl_2]^-$ to $[Ni(dppe)_2]^+$ *via* the $1/K_1$ chemical step. The efficiency of this step is likely a consequence of the relatively low charging current of 1 mA in which ample time is given for ligand transfer to occur. Further studies are underway to vary the applied current and understand the impacts of ligand transfer on RFB cycling.

Comparing the $[Ni(dmpe)_2]^{2+}$ and $[Ni(dppe)_2]^{2+}$ complexes in the context of an RFB, they both achieve $2e^-$ storage at a single charge–discharge potential in the presence of TBACl electrolyte and both benefit from a negative voltage increase due to chloride coordination. The dmpe complex has a larger charge–discharge potential at -1.50 V, compared to -0.98 V for the dppe complex. However, the dppe complex is much more stable over multiple charge–discharge cycles. Both complexes exhibit moderate solubility in MeCN in the Ni(II) oxidation states, 130 mM for $[Ni(dmpe)_2]^{2+}$ and 6 mM for $[Ni(dppe)_2]^{2+}$ with 0.2 M $TBAPF_6$. These solubilities increase to 320 mM and 10 mM with 0.2 M TBACl, respectively. Coupling these solubilities with the $2e^-$ storage capabilities of both complexes, theoretical maximum charge densities of 17.2 A h L^{-1} for $[Ni(dmpe)_2]^{2+}$ and 0.5 A h L^{-1} for $[Ni(dppe)_2]^{2+}$ can be calculated.

The storage of $2e^-$ at a single potential *versus* sequential $1e^-$ redox events is an important distinction. The former offers the advantage of a consistent charge–discharge voltage profile and a greater energy efficiency by compressing the voltage profile over a narrower range. However, developing such redox couples with inorganic complexes requires ECE redox cycles which undergo coordination changes in their chemical steps. This can result in inefficiencies in the redox cycle or can invite degradation pathways due to changes in coordination environment. Understanding and controlling mechanisms for two-electron redox cycles is therefore critically important to developing multi-electron inorganic redox-active molecules for applications in RFBs.

Data availability

The data supporting this article have been included as part of the ESI.†

Conflicts of interest

There are no conflicts to declare.

References

1 Z. Zhu, T. Jiang, M. Ali, Y. Meng, Y. Jin, Y. Cui and W. Chen, *Chem. Rev.*, 2022, **122**(22), 16610–16751.
2 T. M. Gür, *Energy Environ. Sci.*, 2018, **11**(10), 2696–2767.
3 B. Dunn, H. Kamath and J.-M. Tarascon, *Science*, 2011, **334**, 928–935.
4 Z. Yang, J. Zhang, M. C. W. Kintner-Meyer, X. Lu, D. Choi, J. P. Lemmon and J. Liu, *Chem. Rev.*, 2011, **111**(5), 3577–3613.
5 L. Li, S. Kim, W. Wang, M. Vijayakumar, Z. Nie, B. Chen, J. Zhang, G. Xia, J. Hu, G. Graff, J. Liu and Z. Yang, *Adv. Energy Mater.*, 2011, **1**(3), 394–400.
6 J. Noack, N. Roznyatovskaya, T. Herr and P. Fischer, *Angew. Chem., Int. Ed.*, 2015, **54**(34), 9776–9809.
7 M. Lopez-Atalaya, G. Codina, J. R. Perez, J. L. Vazquez and A. Aldaz, *J. Power Sources*, 1992, **39**(2), 147–154.
8 K. Lourenssen, J. Williams, F. Ahmadpour, R. Clemmer and S. Tasnim, *J. Energy Storage*, 2019, **25**, 100844.
9 C. Xie, Y. Duan, W. Xu, H. Zhang and X. Li, *Angew. Chem., Int. Ed.*, 2017, **56**(47), 14953–14957.
10 B. Huskinson, M. P. Marshak, C. Suh, S. Er, M. R. Gerhardt, C. J. Galvin, X. Chen, A. Aspuru-Guzik, R. G. Gordon and M. J. Aziz, *Nature*, 2014, **505**(7482), 195–198.
11 K. Lin, Q. Chen, M. R. Gerhardt, L. Tong, S. B. Kim, L. Eisenach, A. W. Valle, D. Hardee, R. G. Gordon, M. J. Aziz and M. P. Marshak, *Science*, 2015, **349**(6255), 1529–1532.
12 S.-H. Shin, S.-H. Yun and S.-H. Moon, *RSC Adv.*, 2013, **3**(24), 9095–9116.
13 Md. M. R. Mazumder, N. Dalpati, P. R. Pokkuluri and B. H. Farnum, *Inorg. Chem.*, 2022, **61**(48), 19039–19048.
14 H. Jude, J. A. Krause Bauer and W. B. Connick, *J. Am. Chem. Soc.*, 2003, **125**(12), 3446–3447.
15 K. M. Waldie, S. Ramakrishnan, S.-K. Kim, J. K. Maclaren, C. E. D. Chidsey and R. M. Waymouth, *J. Am. Chem. Soc.*, 2017, **139**(12), 4540–4550.
16 D. T. Pierce and W. E. Geiger, *J. Am. Chem. Soc.*, 1989, **111**(19), 7636–7638.
17 D. E. Berning, B. C. Noll and D. L. DuBois, *J. Am. Chem. Soc.*, 1999, **121**(49), 11432–11447.
18 M. P. McLaughlin, T. M. McCormick, R. Eisenberg and P. L. Holland, *Chem. Commun.*, 2011, **47**(28), 7989–7991.
19 K. J. Lee, K. M. Lodaya, C. T. Gruninger, E. S. Rountree and J. L. Dempsey, *J. Chem. Sci.*, 2020, **11**(36), 9836–9851.
20 M. A. Gross, A. Reynal, J. R. Durrant and E. Reisner, *J. Am. Chem. Soc.*, 2014, **136**(1), 356–366.